European Journal of Applied Physics
ISSN: 2684-4451

Photoluminescence Properties of InGaN/InGaN MQWs with Different Electron Injection Layers

Remziye Tülek

***Abstract* — The structural and optical properties of InxGa1-xN/InyGa1-yN multi quantum well (MQW) light emitting devices with/without electron injection layers were studied. The samples with electron injection layer consist of step-graded (GIE) and two step staircase (SEI) electron injection layer between n-type GaN and MQWs active region. Edge and screw type of dislocation densities were deduced from High Resolution X-Ray Diffraction (HR-XRD) curves and no significant difference were realized. The zeroth and higher order satellite peaks were more clearly observed in the sample without electron injection layer. Optical characterization was carried out by temperature dependent photoluminescence (PL) technique. It was found that the PL densities of samples with step-graded and two step-staircase electron injection layers had almost two times lower temperature dependence compared to the reference sample without electron injection layer. On the other hand, the line width of the photoluminescence peak associated with MQWs is much narrower at low temperature for sample without electron injection layer than the other two samples.**

***Keywords* —** Electron Injector Layer, InGaN, LED, Photoluminescence.

I. Introduction

Visible and near ultraviolet (UV) In(Al)GaN/GaN MQW-LEDs are being studied due to their wide range of applications[1]-[7]. Despite the commercial success of InGaN-based light emitting devices, there is still controversy about the fundamentals of the responsible recombination mechanism [8]. The emissions observed in InGaN-based light emitting devices are greatly influenced by the quantum confined Stark effect (QCSE) due to the strong piezoelectric field [9] and carrier localization [10] due to In fluctuations. In addition, possible defects in InGaN quantum wells and/or indium phase separation [10], [11] involving nanosized clusters surrounded by large-bandgap material that behave like quantum dots (QDs) [12] are also considered as mechanisms responsible for emissions in InGaN quantum well structures. To minimize the effect of QCSE along with ballistic and quasi-ballistic electron overflow through the MQW active region an additional low In content InGaN is usually inserted in the form of staircase, step-graded, or continuously graded electron injector layer between n-GaN and the MQW region of the LED structure [13]. This additional layer introduced under the active region in LED structure is also expected to lead to reduction of stress and improve quality of the QW.

The "S-shaped" type of anomalous temperature behavior of the photoluminescence (PL) emission peak is generally considered to be a typical feature of the localization. Alternative explanations for this unusual behavior have also been proposed [14]-[17]. For example, it has been argued that the temperature-dependent photoluminescence peak energy exhibiting an S-shape behavior could be explained by temperature-dependent carrier recombination dynamics due to inhomogeneity and carrier localization in the InGaN/GaN MQWs [18] and InGaN epilayer [19]. On the other hand, a large Stokes shift of PL peak position relative to the absorption edge is often observed in InGaN/GaN QW structure. The physical origin of the observed Stokes shift observed in InGaN ternary alloy system was primarily attributed to the effects of alloy composition fluctuations [20], [21]. The effect of a piezoelectric field induced by a strain resulting in QCSE in a well layer was also considered an alternative mechanism for the observed S-shape behavior [22]. The models of carrier localization and QCSE can provide certain explanations for the observed optical phenomena in InGaN/GaN QW structures [23].

In this paper, the structural and optical properties of three different $In_xGa_{1-x}N/In_yGa_{1-y}N$ multi-quantum well light emitting diode structures with step-graded (sample A), two step-staircase (sample B) and without any (sample C as reference) electron injection layers were determined by High Resolution X-ray Diffraction and temperature-dependent photoluminescence measurements.

Submitted on January 23, 2023.
Published on February 20, 2023.
R. Tülek, Department of Physics, Balıkesir University, Turkey.
(corresponding e-mail: baran@balikesir.edu.tr)

II. Experimental Details

$In_xGa_{1-x}N/In_yGa_{1-y}N$ MQW LED structures were grown on c-plane sapphire substrate using Metalorganic Chemical Vapor Deposition (MOCVD) [24]. The layered structures and calculated energy band profiles of devices coded as sample A, B and C are shown in Fig. 1. The potential profiles and carrier concentrations of structures assumed to grow pseudomorphically were calculated by self-consistent solution of one-dimensional Schrödinger-Poisson equations. The active regions of all samples were deposited on ~4 μm thick n-GaN templates. Sample A and B have 4 and 6 periods of 3 nm thick $In_{0.15}Ga_{0.85}N$ wells and $In_{0.06}Ga_{0.94}N$ barrier layers. Sample C consists of 10 periods of $In_{0.03}Ga_{0.97}N/In_{0.15}Ga_{0.85}N$ MQWs with barrier and well thicknesses of 3 and 8 nm, respectively. Sample A with a 21 nm thick graded electron injection (GEI) layer (7 steps from 4% to 10% in In content) differs from sample B with a two-step ladder electron injection (SEI) (15 nm $In_{0.04}Ga_{0.96}N$) layer. These layers are designed to reduce electron flooding [24]. To improve the quality of the active regions, a 60 nm thick Si-doped $In_{0.01}Ga_{0.99}N$ layer was grown under the electron injection layers. The LED structures were completed with 100 nm thick Mg doped p-GaN cap layers. These devices were designed to operate within the blue/near UV region of the spectrum.

The crystalline quality and dislocation densities of samples were determined by high-resolution X-ray diffraction (HR-XRD). Temperature dependent PL measurements were performed in the temperature range of 10–300 K. A frequency tripled pulse laser emitted at 349 nm were used for excitation. The luminescence collected by suitable lenses were dispersed with a 500 mm spectrometer using 1200 line/mm grating. The dispersed light detected by Intensified Charge Coupled Device (ICCD) camera and plotted by a commercial software.

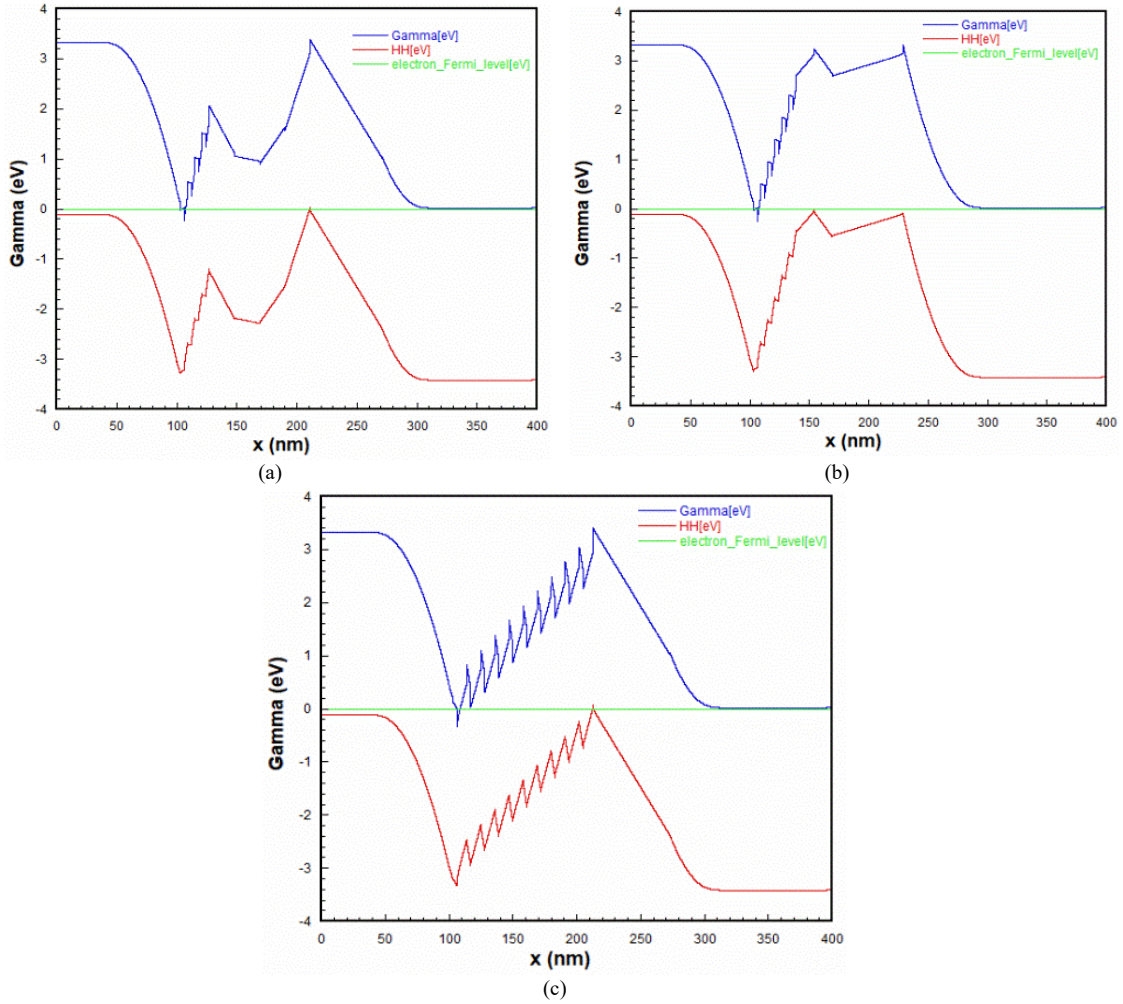

Fig. 1. The layered structures and calculated energy band profiles of sample (a) A; (b) B; (c) C.

III. Experimental Results and Discussion

The XRD data were collected on (002) and (102) reflections with ω-2θ scans. XRD patterns around the (002) reflections is shown in Fig. 2 for samples. The reflection peaks observed at about 34.6° and 41.7° are due to GaN template and sapphire substrate. The peaks or shoulders just observed to the left of this main peak are zero-order reflection peaks corresponding to the average In ratio of all InGaN layers in the structure. The reflection peaks observed at about 34.06°, 33.7°, and 33.9° are from the InGaN quantum wells, for A, B and C respectively. The reflection peaks located symmetrically on the right and left sides of the zero-order peaks are the first and higher order satellite peaks associated with the period of the quantum wells. The observed high-order satellite peaks indicate the structural and interface quality of samples. Screw and edge dislocation densities can be deduced from the FWHM values of the symmetric (002) and asymmetric (102) XRD curves using (1) and (2) [25].

$$D_{screw} = \frac{\beta^2(0002)}{9b_{screw}^2} \quad (1)$$

$$D_{edge} = \frac{\beta^2(1012)}{9b_{edge}^2} \quad (2)$$

where β is the FWHM obtained from XRD rocking curves.

The lengths of Burger vectors for edge and screw types of dislocations were calculated as $b_{edge} = 0.3189$ nm and $b_{screw} = 0.5185$ using the equations $b = \frac{1}{3}\langle 11\bar{2}0\rangle(\langle a\rangle)$ and $b = \langle 0001\rangle(\langle c\rangle)$, respectively. Using Eq.1, the edge and screw dislocation densities were calculated to be 3.8×10^8 and 9.1×10^7 (for sample A), 9.6×10^8 and 1.4×10^8 (for sample B) and 7.6×10^8 and 1.1×10^8 cm^{-2} (for sample C). No significant difference was observed in the dislocation densities in samples A and B compared to the reference sample.

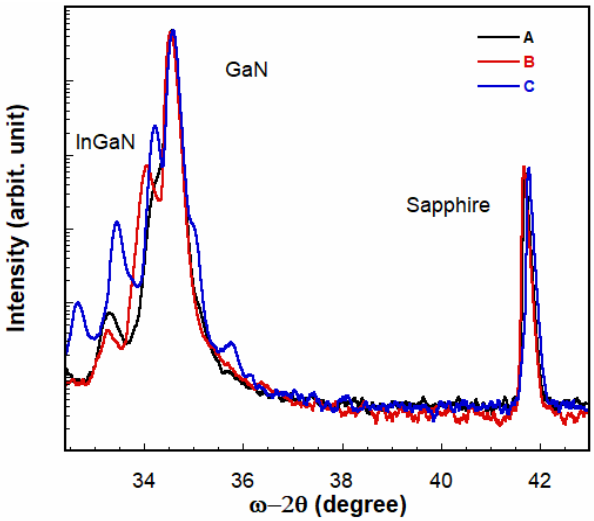

Fig. 2. HR-XRD (002) ω-2θ scans of all of samples.

Fig. 3 shows the PL spectra taken in the temperature range of 10 to 300 K for all samples. The excitation intensity was kept low at 30 W/cm^2 to avoid overheating and high excitation effects. At 10 K, the peaks observed at 2.90, 2.86, and 2.96 eV are related to the transitions in active region of devices with InGaN/InGaN MQWs.

The peaks observed in the 3.2-3.3 eV spectral range for sample A correspond to donor-acceptor-pair (DAP) and/or band-to-acceptor transitions. This peak was not seen for sample B and weakly observed for sample C. The yellow luminescence (YL) at 2.1-2.2 eV range were observed for all samples. The main peaks associated with MQWs were observed at room temperature as 2.88, 2.82, and 2.93 eV for samples A, B, and C, with a redshift of 20 meV, 40 meV, and 30 meV, respectively. No S-like behavior was observed in our samples, representing the segregation effect. The periodic oscillation with a period of approx. 30 meV seen in all spectra are due to the interference effect. The main difference in PL spectra between sample C and, other two is the linewidth of the main emission peaks. It is much larger for samples A and B than C, indicating strength of the longitudinal phonon interactions. The brooding of the spectra is due to phonon-replicas of the main peaks. As seen in Fig. 3, the PL intensities decrease as the temperature increase at different rates.

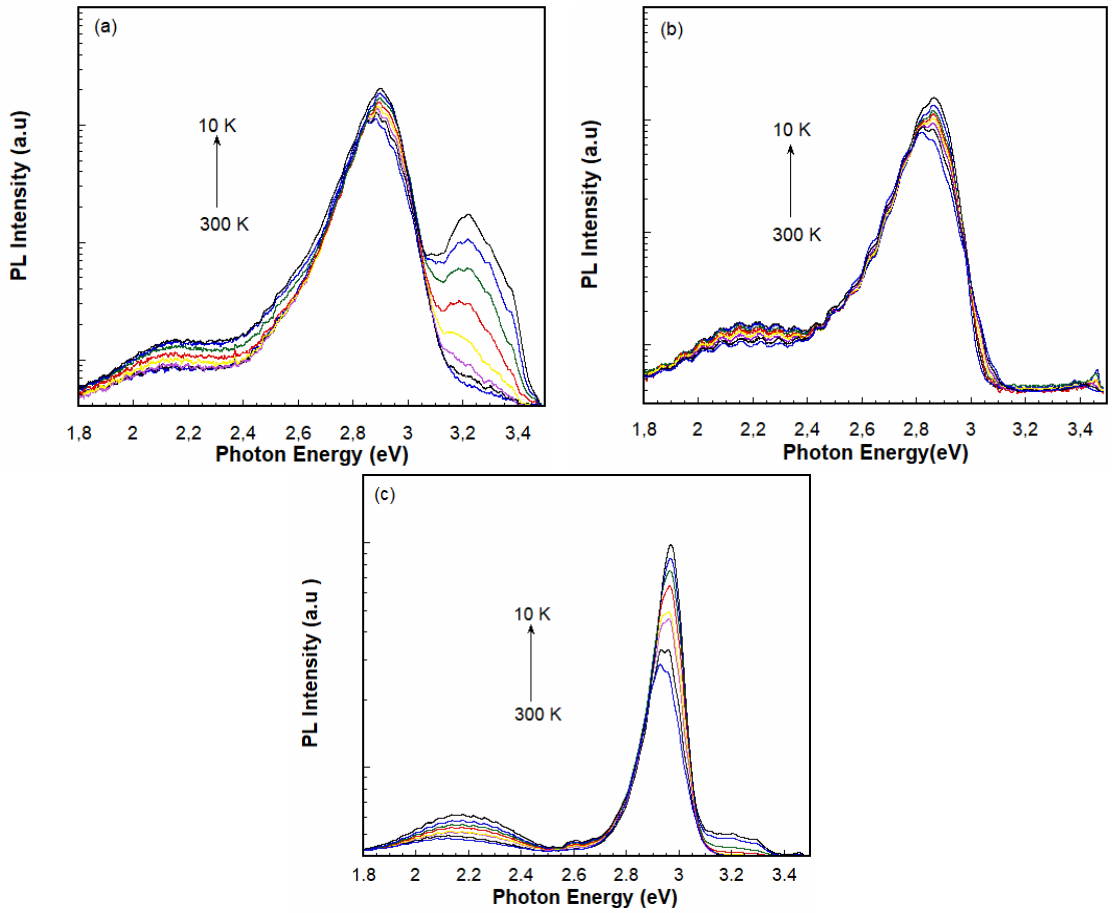

Fig. 3. The PL spectra for (a) sample A, (b) B and (c) C between 10 to 300 K.

Fig. 4a shows the inverse temperature dependent normalized PL intensity. They were fitted by the dual-channel Arrhenius equation given in (3) [26].

$$I(T) = \frac{I_0}{1+A_1 \exp\left(-\frac{E_1}{k_B T}\right)+A_2 \exp\left(-\frac{E_2}{k_B T}\right)} \quad (3)$$

where I_0 is the PL intensity as the temperature goes to zero,
E_1 and E_2 are energies of thermally activated non-radiative recombination channels,
A_1 and A_2 are related to capture rates, and k_B is Boltzmann's constant.

The observed thermal quenching of the PL intensities is probably due to thermionic emission of photocarriers over the confining potential caused by alloy and/or interface fluctuations. Thus, the activation energies can be considered to correspond to the strength of the potential fluctuations present in the emission regions. PL intensities decreases rather small at low temperatures but more gradually at higher temperatures for all samples. These results indicate that there are two nonradiative recombination centers that are responsible for low-and high-temperature regimes. By fitting using (3), the thermal activation energies and corresponding rate constants for low and high temperature regime were deduced. The low temperature activation energies of 13 meV, 12.5 meV and 10 meV were obtained with low-rate constants of 1.0, 0.6 and 0.5 for sample A, B, and C, respectively. Since most exciton binding energies of donor-bound impurities are in the order of ten meV, low-temperature activation energies are expected to be related to carriers released by the impurities and captured by nonradiative recombination centers in InGaN/InGaN quantum wells. As the temperature increases further, another nonradiative recombination channel with the thermal activation energies of 197 meV, 159 meV and 155 meV become apparent for samples A, B, and C, respectively. Since these energies are in the order of confined potential of quantum wells, the carriers may overcome the potential barriers and captured by nonradiative recombination centers. The constants related to the nonradiative capture rates with the values of 56, 75 and 85 for samples A, B and C, respectively are much faster than low temperature ones.

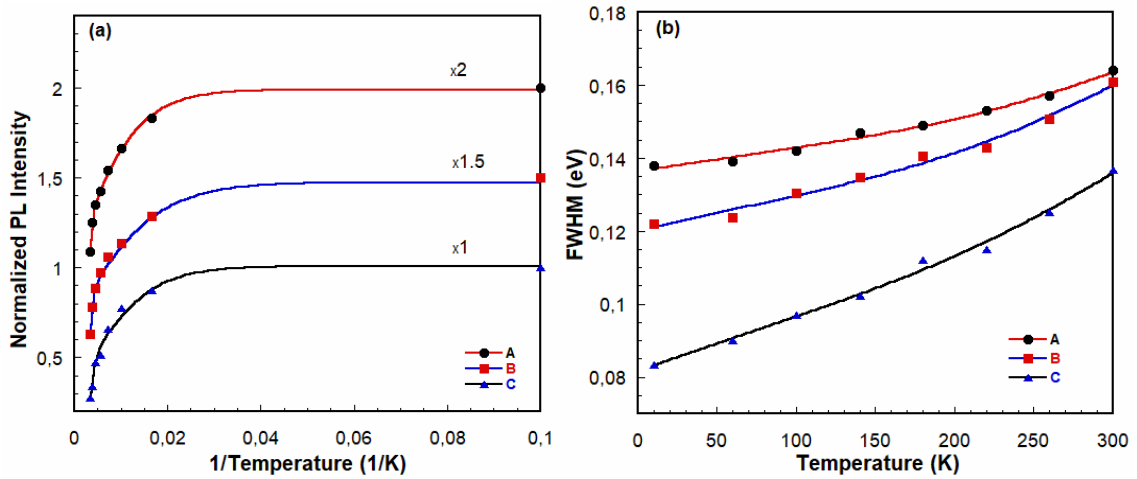

Fig. 4. (a) Normalized peak PL intensities as a function of an inverse temperature for all samples. The normalized PL intensities were randomly scaled to clearly distinguish the plots). (b) Temperature dependent FWHM of the PL spectra for all samples.

Fig. 4b shows FWHM of the PL spectra as a function of temperature. The FWHM of quantum well emissions obtained by applying the multiple Gaussian fitting to the measured spectra. As seen from the figure, the FWHM increases with increasing temperature with different rates at low and high temperature regimes for all samples. The luminescence line width may generally compose of a temperature independent inhomogeneous and a temperature-dependent homogeneous parts. The inhomogeneous part is mainly because of the interface roughness and alloy disorder in strained quantum well structure. The homogenous part is due to the scattering by acoustic and longitudinal optical phonons. The overall temperature dependent FWHM is often described by (4) [27].

$$\Gamma(T) = \Gamma(0) + \gamma_{LA} T + \frac{\Gamma_{LO}}{\exp\left(\frac{E_{LO}}{k_B T}\right)-1} \quad (4)$$

where $\Gamma(0)$ is the inhomogeneous broadening constant,
γ_{LA} is related to exciton-acoustic phonon coupling,
Γ_{LO} is the parameter which determine the strength exciton-LO-phonon interactions,
and E_{LO} is the LO-phonon energy which is taken as about 88 meV in the fitting.

From Fig. 4b, the FWHMs increase linearly up to 150 K, where acoustic phonon scattering predominates. Above 150 K, relatively rapid increase observed in FWHM values represent the dominance of longitudinal optical phonons due to the increasing optical phonon population. The total line width is indicative of optical and acoustic phonon scatterings.

IV. Conclusion

We have studied the photoluminescence properties of three samples designed as light emitting diodes operating in the visible region of spectrum. The effect of step-graded and step staircase electron injection layers grown under the active emission regions composed of InxGa1-xN/InyGa1-yN was studied in detail by analyzing temperature dependence of PL measurements. Sample C without any electron injection layer was used as a reference. From these analyses, it was found that the PL densities of samples with step-graded and step-staircace electron injection layers had almost two times lower temperature dependence compared to the reference sample, as evidenced by their non-radiative capture rates. On the other hand, the FWHMs of sample A and B are almost 2 times wider compared to reference sample at 10K. They increase less steeply, indicating less exciton-phonon scattering than in the reference sample. The ratio decreases to 1.14 at room temperature. In the structural analysis, the satellite peaks were more clearly seen in reference sample, and no significant difference was observed in the dislocation densities in samples A and B compared to the reference sample.

Acknowledgment

Author thanks Hadis MORKOÇ, Ümit ÖZGÜR and Vitaliy Avrutin from Virginia Commonwealth University for providing the samples used in this study, and Ali TEKE from Balıkesir University for valuable suggestions on manuscript.

REFERENCES

[1] Nakamura S, Fasol G, Pearton SJ. *The Blue Laser Diode: The Complete Story* (2nd updated and extended ed. 2000). Springer: 2000.
[2] Ponce FA, Bour DP. (1997). Nitride-based semiconductors for blue and green light-emitting devices. *Nature,* 1997; 386(6623): 351–359. https://doi.org/10.1038/386351a0.
[3] Ozbay E, Biyikli N, Kimukin I, Kartaloglu T, Tut T, Aytur O. High performance solar-blind photodetectors based on $Al_xGa_{1-x}N$ heterostructures. *IEEE Journal of Selected Topics in Quantum Electronics*, 2004;10(4):742-751. http://dx.doi:10.1109/JSTQE.2004.831681.
[4] Teke A, Dogan S, He L, Huang D, Yun F, Mikkelson M, Morkoç H, Zhang SK, Wang WB, Alfano RR. p-GaN-i-GaN/AlGaN multiple-quantum well n-AlGaN back-illuminated ultraviolet detectors. *J. Electronic Materials*, 2003; 32(5): 307-311. https://doi:10.1007/s11664-003-0149-4.
[5] Tut T, Gokkavas M, Inal A, Ozbay E. $Al_xGa_{1-x}N$ based avalanche photodiodes with high reproducible avalanche gain. *Appl. Phys. Lett*, 2007; 90(16): 163506. https://doi.org/10.1063/1.2724926.
[6] Adivarahan V, Fareed Q, Srivastava S, Katona T, Gaevski M, Khan A. Robust 285 nm Deep UV Light Emitting Diodes over Metal Organic Hydride Vapor Phase Epitaxially Grown AlN/Sapphire Templates. *Jpn. J. Appl. Phys*, 2007; 46(23): 537-539. https://doi:10.1143/JJAP.46.L537.
[7] Okamoto K, Niki I, Shvartser A, Narukawa Y, Mukai T, Scherer A. Surface-plasmon-enhanced light emitters based on InGaN quantum wells. *Nature Materials*, 2004; 3(9): 601-605. https://doi:10.1038/nmat1198.
[8] Kuzmík J. Power Electronics on InAlN/(In)GaN: Prospect for a record performance, *IEEE Electron Device Lett*. 2001; 22(11): 510. https://doi.org/10.1109/55.962646.
[9] Bai J, Wang T and Sakai S Study of the strain relaxation in InGaN/GaN multiple quantum well structures. *J. Appl. Phys*, 2001; 90(4): 1740. https://doi:10.1063/1.1389330.
[10] Narukawa Y, Kawakami Y, Fujita S, Fujita S. Recombination dynamics of localized excitons in $In_{0.20}Ga_{0.80}N$-$In_{0.05}Ga_{0.95}N$ multiple quantum wells. *Phys. Rev. B*, 1997; 55(4): 1938. https://doi:10.1103/physrevb.55.r1938.
[11] Chichibu S, Azuhata T, Sota T, Nakamura S. Luminescences from localized states in InGaN epilayers. *Appl. Phys. Lett*., 1997; 70(21): 2822. https://doi:10.1063/1.119013.
[12] Lin YS, Ma KJ, Hsu C, Feng SW, Cheng YC, Liao CC, Yang CC, Chou CC, Lee CM, Chyi JI. Dependence of composition fluctuation on indium content in InGaN/GaN multiple quantum wells. *Appl. Phys. Lett*, 2000; 77(19): 2988. https://doi:10.1063/1.1323542.
[13] Sheremet V, Gheshlaghi N, Sözen M, Elçi M, Sheremet N, Aydınlı A, Altuntaş I, Ding K, Avrutin V, Özgür Ü, Morkoç H. InGaN stress compensation layers in InGaN/GaN blue LEDs with step graded electron injectors. *Superlattices and Microstructures*, 2018; 116. https://doi.org/10.1016/j.spmi.2018.02.002.
[14] Taliercio T, Lefebvre P, Gallart M, Morel A. Optical properties of group-III nitride quantum wells and quantum boxes. *Journal of Physics: Condensed Matter*, 2001; 13(32): 7027-7042. https://doi:10.1088/0953-8984/13/32/310.
[15] Cho Y-H, Gainer GH, Fischer AJ, Song JJ, Keller S, Mishra UK, DenBaars SP. "S shaped" temperature dependent emission shift and carrier dynamics in InGaN/GaN multiple kuantum wells. *Appl. Phys. Lett*, 1998;73:1370. https://doi:10.1063/1.122164.
[16] Eliseev PG, Perlin P, Lee J, Osinski M. "Blue" temperature-induced shift and band-tail emission in InGaN-based light sources. *Appl. Phys. Lett*, 1997; 71: 569. https://doi.org/10.1063/1.119797.
[17] Teo KL, Colton JS, Yu PY, Weber ER, Li MF, et al. An analysis of temperature dependent photoluminescence line shapes in InGaN. *Appl. Phys. Lett*, 1998; 73(12): 1697. https://doi.org/10.1063/1.122249.
[18] Wang T, Bai J, Sakai S, Ho JK. Investigation of the emission mechanism in InGaN/GaN-based light-emitting diodes. *Appl. Phys. Lett*, 2001; 78(18): 2617. https://doi:10.1063/1.1368374.
[19] Kanemitsu Y, Tomita K, Hirano D, Inouye H. Temperature dependence of exciton localization dynamics in $In_xGa_{1-x}N$ epitaxial films. *Appl. Phys. Lett*. 2006; 88: 121113. https://doi.org/10.1063/1.2187954.
[20] Huang YH, Cheng CL, Chen TT, Chen YF. Tsen KT. Studies of Stokes shift in Inx Ga1-xN alloys. *J. Appl. Phys*, 2007; 101(10): 103521. https://doi.org/10.1063/1.2724797.
[21] Sasaki C, Naito H, Iwata M, Kudo H, Yamada Y, Taguchi T, Jyouichi T, Okagawa H, Tadatomo K, Tanaka H. Temperature dependence of Stokes shift in InGaN epitaxial layers. *J. Appl. Phys*, 2003; 93: 1642. https://doi.org/10.1063/1.1533093.
[22] Riblet P, Hirayama H, Kinoshita A, Hirata A, Sugano T, Aoyagi Y. Determination of photoluminescence mechanism in InGaN quantum wells. *Appl. Phys. Lett*, 1999; 75: 2241. https://doi.org/10.1063/1.124977.
[23] Bell A, Christen J, Bertram F, Ponce FA, Marui H, Tanaka S. Localization versus field effects in single InGaN quantum wells. *Appl. Phys. Lett*, 2004; 84: 58. https://doi.org/10.1063/1.1638880.
[24] Can N, Okur S, Monavarian M, Zhang F, Avrutin V, Morkoç H, Teke A, Özgür Ü. Active region dimensionality and quantum efficiencies of InGaN LEDs from temperature dependent photoluminescence transients. *Proc. of SPIE*, 2015; 9363: 93632U. https://doi: 10.1117/12.2179637.
[25] Arslan E, Özturk MK, Teke A, Özcelik S, Özbay E. Buffer optimization for crack-free GaN epitaxial layers grown on Si (111) substrate by MOCV. *J. Phys. D: Appl. Phys*, 2008; 41: 258. https://doi:10.1088/0022-3727/41/15/155317.
[26] Park J-Y, Lee J-H, Jung S, Ji T. InGaN/GaN-based green-light-emitting diodes with an inserted InGaN/GaN-graded superlattice layer. *Phys. Status Solidi A*, 2016; 213: 1610–1614. https://doi: 10.1002/pssa.201533092.
[27] Gotz W, Johnson NM, Chen C, Liu H, Kuo C, Imler W. Activation energies of Si donors in GaN. *Appl. Phys. Lett*, 1996; 68: 3144. https://doi.org/10.1063/1.115805.